Inorganic Chemistry

Article

pubs.acs.org/IC

Crystal Structures of Al−Nd Codoped Zirconolite Derived from Glass Matrix and Powder Sintering

Chang-Zhong Liao,[†] Kaimin Shih,*[,†] and William E. Lee[‡]

[†]Department of Civil Engineering, The University of Hong Kong, Pokfulam Road, Hong Kong SAR

[‡]Department of Materials and Centre for Nuclear Engineering, Imperial College London, London SW7 2AZ, U.K.

Supporting Information

ABSTRACT: Zirconolite is a candidate host for immobilizing long-lived radionuclides. Zirconolite-based glass-ceramics in the CaO-SiO_2-Al_2O_3-TiO_2-ZrO_2-Nd_2O_3-Na_2O matrix are a potential waste form for immobilizing actinide radionuclides and can offer double barriers to immobilize radioactive elements. However, the X-ray diffraction patterns of the zirconolite derived from the glass matrix (glass ceramic, GC) are significantly different from those prepared by powder sintering (PS). In this Article, the crystal structures of Al−Nd codoped zirconolite grown via the glass matrix route and the powder sintering route are investigated in detail. Two samples of Al−Nd codoped zirconolite were prepared: one was grown from a CaO-SiO_2-Al_2O_3-TiO_2-ZrO_2-Nd_2O_3-Na_2O glass matrix, and the other was prepared with a $Ca_{0.75}Nd_{0.25}ZrTi_{1.75}Al_{0.25}O_7$ composition by powder sintering. The samples were then characterized using powder X-ray diffraction (PXRD), scanning electron microscopy (SEM), transmission electron microscopy−energy dispersive X-ray spectroscopy (TEM-EDX), and selected area electron diffraction (SAED). The chemical composition of the 100−500 nm zirconolite crystals grown from a glass matrix was determined by TEM-EDX to be $Ca_{0.83}Nd_{0.25}Zr_{0.85}Ti_{1.95}Al_{0.11}O_7$. PXRD and SAED results showed that these two Al−Nd codoped zirconolite phases were crystallized in space group $C12/c1$. The HRTEM images and SAED results showed that there were heavy stacking faults in the zirconolite crystals grown from the glass matrix. In contrast, far fewer defects were found in the zirconolite crystals prepared by powder sintering. The split-atom model was adopted for the first time to construct the Al−Nd codoped zirconolite structure grown from glass during the Rietveld refinement. The isostructural method assisted by Rietveld refinement was used to resolve the Al−Nd codoped zirconolite structures prepared by different methods. The occupancies of the cation sites were identified, and the distribution behavior of Nd^{3+} was further investigated. The results indicate that the heavy stacking faults may lead to substantial differences in the Al−Nd codoped zirconolite structures prepared by these two fabrication routes.

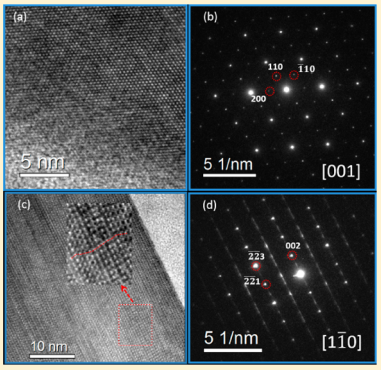

INTRODUCTION

A key factor in designing nuclear waste forms is the existence of natural analogues that contain radionuclides and that are thermodynamically stable over geological time.[1] Up to now, many nuclear waste forms have been proposed to immobilize high level nuclear waste, and these forms can be classified into three types, i.e., glass, ceramic, and glass-ceramic.[2] The glass waste forms have been used to dispose the nuclear waste in many countries due to its wide range of radionuclide incorporation and good chemical durability.[3,4] In the ceramic waste forms, single-crystalline phases such as zirconolite, zircon, cubic-zirconia, apatite, and pyrochlore are potential host phases for actinides.[5] For glass-ceramic, it can combine the advantages of glass and ceramic to avoid their drawbacks.[2] Thus, the residual glass can immobilize a wide range of radionuclides, while the crystalline phase further incorporates actinides into the specific crystal structures.[3,4] In France, zirconolite-based glass-ceramics were proposed and designed by Caurant and co-workers as a double-barrier matrix for the immobilization of minor actinides.[6−11]

Zirconolite exists in nature containing impurity elements, including lanthanides, actinides, Nb, and Fe.[12] It has been intensively studied since the 1970s, when it was proposed as one of the phases in an artificial rock (Synroc) for nuclear waste immobilization.[13] Synroc is made up of hollandite, perovskite, and zirconolite. Zirconolite and perovskite are the main host phases for lanthanides and actinides.[14] Because of its higher chemical durability and radiation tolerance, zirconolite was favored in many studies as a waste form candidate for immobilizing minor actinides.[14,15] With an ideal stoichiometry of $CaZrTi_2O_7$, zirconolite is a fluorite-type derived superstructure.[16] In the literature, five zirconolite polytypes have been observed in natural and synthetic samples. These are zirconolite-2M (monoclinic polytype),[13] zirconolite-3T (trigonal polytype),[17] zirconolite-3O (orthorhombic polytype),[18] zirconolite-4M (monoclinic polytype),[19] and zirconolite-6T (trigonal polytype).[20] The crystal structures of many compounds related to the above polytypes have been solved,

Received: April 18, 2015
Published: July 23, 2015

DOI: 10.1021/acs.inorgchem.5b00847
Inorg. Chem. 2015, 54, 7353−7361

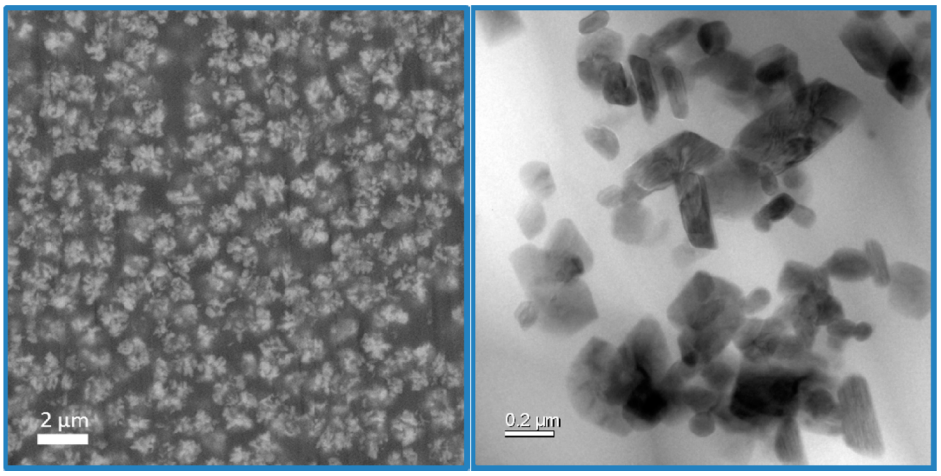

Figure 1. Backscattered SEM (left) and bright-field TEM (right) images of the Zir-GC sample prepared after nucleation at 810 °C for 2 h and crystal growth at 1050 °C for 2 h.

except that of zirconolite-6T. The 6T structure was only reported by Smith and Lumpkin[20] and deduced from the results of high resolution electron microscopy (HRTEM) and selected area electron diffraction (SAED). However, no further structural details are provided in the literature. All of these polytypes are constructed by combining hexagonal tungsten bronze (HTB) and Ca−Zr layers, and are defined by different stacking numbers and styles.[19] For instance, 2M-zirconolite consists of two HTB layers and two Ca−Zr layers, and the 3T structure has three HTB layers and three Ca−Zr layers. The appearance of these polytypes also depends on the incorporated elements and the sintering temperature.[20] Triyacharoen[21] used a charge-compensation mechanism and the cation radius ratio of substitutes to discuss and predict the solubility limits of the elements incorporated in zirconolite polytypes. In the rare earth element (REE)-doped zirconolite system, the 2M structure often appears at low substitute levels, while the 4M structure tends to form at high REE substitute levels. For Nd-doped zirconolite, differences in the Nd content may lead to 2M, 3T, or 4M structures.[20] For Al−Nd codoped zirconolite ($Ca_{1-x}Nd_xZrTi_{2-x}Al_xO_7$) in samples derived by the powder sintering method, the structure is suggested to be 2M when $0 \leq x \leq 0.6$ and 3O when $0.65 \leq x \leq 0.8$.[6]

In the zirconolite-based glass-ceramic matrix, a single crystalline phase of zirconolite was obtained in a bulk sample by controlled crystallization (nucleation and crystal growth) at 1050 °C in a SiO_2-Al_2O_3-CaO-ZrO_2-TiO_2-Na_2O-REE_2O_3 glass matrix.[10] The X-ray diffraction (XRD) patterns of the obtained zirconolite codoped by REE and Al can be indexed to the 2M structure. However, far fewer diffraction peaks were observed for REE- and Al-doped zirconolite grown from a glass matrix compared with that crystallized through powder sintering.[6,10,22,23] Loiseau et al. explained this phenomenon by assuming that the Ca^{2+} and Zr^{4+} in the Ca−Zr layers was completely disordered in the products derived from the glass matrix.[6] No further structural details about REE- and Al-doped zirconolite grown from a glass matrix are available in the literature. In addition, only when the temperature reached 1200 °C for a sufficient crystal size (2000 nm−5000 nm) was the chemical composition of the zirconolite crystals grown from a glass matrix reported via electron scanning microscopy−energy dispersive X-ray spectroscopy (SEM-EDX).[10] The chemical compositions of the zirconolite crystals crystallized at 1050 °C have not been determined by SEM-EDX due to the small crystal sizes. Results from Caurant[7] revealed that the amount of zirconolite phase in the 1050 °C sample is much higher than that in the 1200 °C sample. This result indicates that the product crystallized at 1050 °C is more suitable for nuclear waste immobilization. Moreover, the precise determination of crystal chemical compositions is highly beneficial for discussing their loading capacity of radionuclides, together with the partitioning ratio of radionuclides between crystalline and glass phases. Therefore, it is essential to obtain the chemical compositions of zirconolite crystals grown at 1050 °C.

Furthermore, the microstructure plays an important role in the performance of resisting radiation attacks which intensely affects the properties (such as mechanical properties, thermal conductivity, and leaching behavior) of nuclear waste forms.[14] Studies pointed out that the defects observed in the zirconolite obtained via a ceramic route may assist the radiation tolerance.[5] In Shen's model,[24] which was used to describe the radiation tolerance, point defect was found to dramatically increase radiation durability. Calculation from density functional theory with dispersion correction[25] reveals that the binding energy, which was used to determine the formation of the He bubble, varied with different crystallographic sites. In the zirconolite-based glass-ceramics, strong dislocations were observed in the zirconolite crystals. These dislocations may enhance the radiation tolerance as discussed above. However, these dislocations may lead to the change of atomic arrangement, due to the shift of binding energy. Therefore, accurately describing the crystal structure of the zirconolite crystals in glass-ceramics is highly important.

The aim of this Article is to reveal the chemical composition and structural details of zirconolite crystals grown from a glass matrix at 1050 °C. The crystal structure of the zirconolite derived from power sintering was also solved via PXRD analysis for comparison. To achieve these goals, neodymium (Nd) was used as an example of REEs and as a surrogate for Pu, and zirconolite was crystallized from a SiO_2-Al_2O_3-CaO-ZrO_2-TiO_2-Nd_2O_3-Na_2O glass matrix at 1050 °C. Scanning electron microscopy (SEM), HRTEM, EDX, and SAED were also used to characterize the samples. On the basis of the Rietveld refinement technique for powder X-ray diffraction data, the split-atom model and isostructural method were used to

DOI: 10.1021/acs.inorgchem.5b00847
Inorg. Chem. 2015, 54, 7353−7361

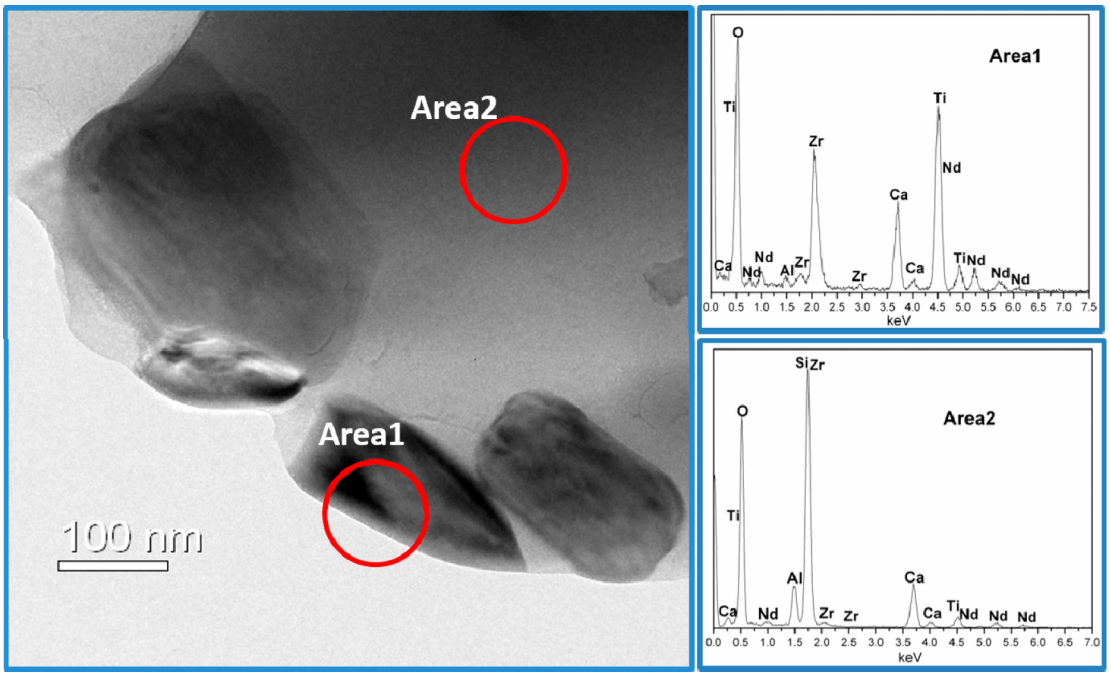

Figure 2. TEM image and EDX results for the corresponding areas of the Zir-GC sample. Area 1 corresponds to the Al–Nd codoped zirconolite crystal and Area 2 to the residual glass.

construct the zirconolite structures grown by the different fabrication routes.

EXPERIMENTAL SECTION

A "Zir-GC" sample was prepared to obtain Al–Nd codoped zirconolite grown from a glass matrix with a chemical composition[22] (by wt %) of SiO_2 (36.07), Al_2O_3 (10.62), CaO (19.18), TiO_2 (15.98), ZrO_2 (11.31), Nd_2O_3 (6.00), and Na_2O (0.84). The parent glass was obtained as follows. Reagent grade oxides (SiO_2, Al_2O_3, TiO_2, ZrO_2, and Nd_2O_3) and carbonates ($CaCO_3$ and $Na_2CO_3{\cdot}10H_2O$) were mixed, melted in a platinum crucible at 1500 °C for 9 h, and then poured into the alumina crucible to be cooled in air. The obtained glass was further ground into powder, remelted at 1500 °C for 5 h, and cooled in air again. The cast parent glass was annealed at 775 °C for 2 h to relieve the internal stresses and then cooled to room temperature. The zirconolite-based glass-ceramic was obtained via a two-step fabrication route as described in the literature:[22] (1) placing the parent glass into a 810 °C preheated furnace for 2 h of nucleation and (2) transferring the sample to a 1050 °C preheated furnace for 2 h of crystal growth. All of the procedures were conducted under atmosphere. Finally, the obtained glass-ceramic was also annealed at 775 °C for 2 h to relieve the internal stresses. For the Al–Nd codoped zirconolite sample synthesized via the powder sintering process (Zir-PS; $Ca_{0.75}Nd_{0.25}ZrTi_{1.75}Al_{0.25}O_7$), $CaCO_3$, ZrO_2, TiO_2, Nd_2O_3, and Al_2O_3 were mixed in their stoichiometric ratio and pressed into a pellet for sintering in air at 1500 °C for 50 h. The product was then ground into powder again to be reprocessed following the same sintering scheme to ensure a complete solid-state reaction and homogeneity.

To be characterized by TEM, the fabricated samples were prepared by mechanical thinning followed by ion beam milling (Fischione Model 1010 Ion Beam Milling). The HRTEM, SAED, and EDX analyses were performed on a FEI Tecnai G2 20 S-TWIN operated at 200 kV. A Hitachi S4800 FEG-SEM, assisted with EDX, was used to observe the sample morphology and chemical composition. The X-ray powder diffraction data were collected using a D8 Advanced Diffractometer (Bruker AXS) with a Lynxeye detector, operating at 40 kV and 40 mA with Cu Kα radiation at room temperature. The 2θ scan range was from 10° to 110° (or 120°) with a step size of 0.02° and a counting time of 1.5 s. The Rietveld refinement was carried out using TOPAS 4.2 software (Bruker AXS GmbH, Germany) with a fundamental parameters approach.

RESULTS AND DISCUSSION

Crystal Size and Chemical Composition of Al–Nd Codoped Zirconolite Grown from a Glass Matrix. After

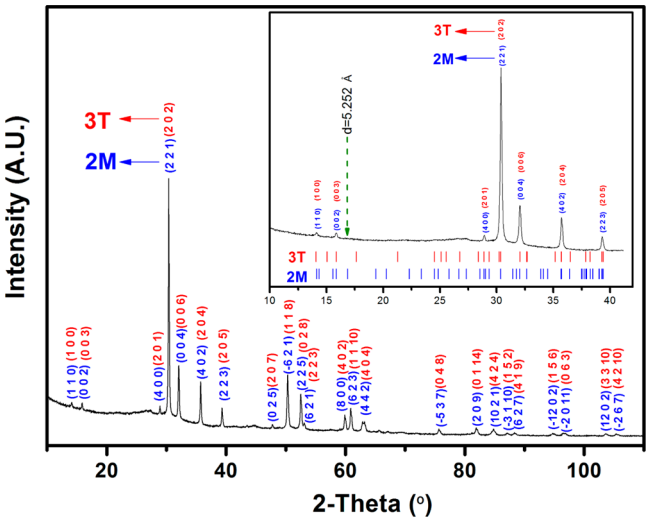

Figure 3. Indexing result for the XRD pattern of the Al–Nd codoped zirconolite phase in the Zir-GC sample. The blue (lower) Miller indices correspond to the case of monoclinic symmetry, and the red (upper) indices to the case of trigonal symmetry. The inset shows the calculated Bragg positions of both the 2 M and 3T structures, and d = 5.252 Å is also indicated.

nucleation at 810 °C for 2 h and crystal growth at 1050 °C for 2 h, the CaO-Al_2O_3-SiO_2-ZrO_2-TiO_2-Nd_2O_3-Na_2O glass was devitrified. Backscattered electron images of the Zir-GC sample showed many ~2 μm clusters immersed and homogeneously distributed in the glass matrix (Figure 1a). TEM further

DOI: 10.1021/acs.inorgchem.5b00847
Inorg. Chem. 2015, 54, 7353–7361

Table 1. Selected Spacing Distances Calculated from the Zirconolite-2M and Zirconolite-3T Structure[a]

zirconolite-2M model a = 12.566 Å b = 7.258 Å c = 11.360 Å β = 100.66°	zirconolite-3T model $a = b$ = 7.256 Å c = 16.746 Å	zirconolite-2M model a = 12.566 Å b = 7.258 Å c = 11.360 Å β = 100.66°	zirconolite-3T model $a = b$ = 7.256 Å c = 16.746 Å
d-spacing (Å)	d-spacing(Å)	d-spacing (Å)	d-spacing(Å)
6.257	6.284	3.451	3.484
6.175	-	3.339	3.329
5.690	5.883	3.262	3.142
5.582	5.582	3.129	3.088
5.252	5.026	3.089	3.042
4.584	4.173	3.074	-
4.374	-	3.042	2.956
3.984	-	2.942	2.942
3.805	-	2.845	-
3.629	3.628	2.816	-
3.581	3.546	2.791	2.791

[a]The "-" represents "not available".

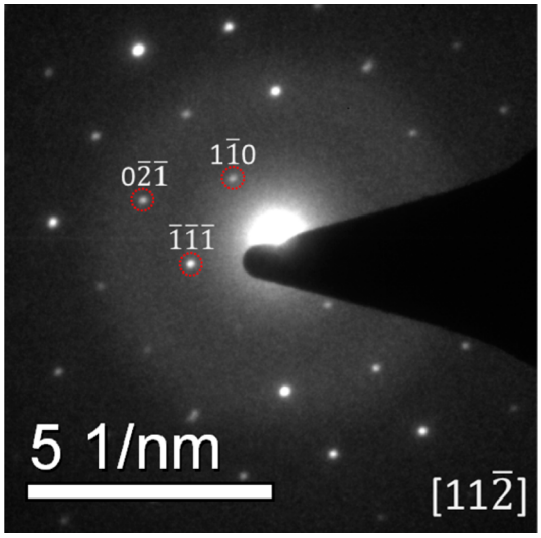

Figure 4. Indexing result for the SAED pattern of the Al–Nd codoped zirconolite in the Zir-GC sample. The characteristic spacing distance for zirconolite-2M was obtained as d = 5.260 Å for the (−1−1−1) plane.

revealed the crystal sizes in the clusters to be 100 to 500 nm. As all of the crystals were small and embedded in the glass matrix (Figure 1b), the use of SEM-EDX to evaluate the chemical composition of the crystals inevitably contains information reflected from the glass matrix, leading to questionable EDX results for the targeted crystals. This is why Loiseau et al.[10] were unable to identify the chemical composition of the crystals crystallized at 1050 °C in this system. Therefore, TEM-EDX analysis was conducted to obtain the chemical compositions of the zirconolite crystals in the Zir-GC sample. In the TEM-EDX analysis, only the crystals located at the edge and not covered by the glass (such as Area 1) were analyzed. This method prevents the interference from the glass and gives a more precise chemical composition result. The EDX spectrum of area 1 (Figure 2), corresponding to the information for the zirconolite crystal, revealed only Ca, Al, Zr, Ti, Nd, and O in the crystal, and Si was not observed. In area 2 (Figure 2), the corresponding residual glass was observed with Ca, Al, Zr, Ti, Nd, Si, and O. Loiseau et al.[10] indicated that Si could not be

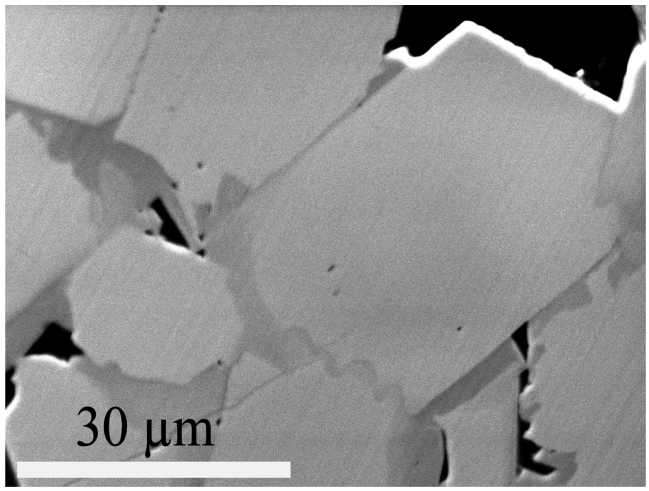

Figure 5. Backscattered SEM image of the Zir-PS sample prepared by powder sintering at 1500 °C for a total of 100 h.

incorporated into zirconolite crystals grown from a CaO-Al_2O_3-SiO_2-ZrO_2-TiO_2-Nd_2O_3-Na_2O glass matrix. Using TEM-EDX analysis, the chemical composition of the zirconolite crystals was determined to be $Ca_{0.83}Nd_{0.25}Zr_{0.85}Ti_{1.95}Al_{0.11}O_7$. The zirconolite crystal composition reported by Loiseau et al.[10] was $Ca_{0.82}Nd_{0.19}Zr_{1.05}Ti_{1.77}Al_{0.17}O_7$, in which the nearly equal amounts of Nd and Al were used to indicate a charge compensation between the occupancy of Ca sites by Nd and the occupancy of Ti sites by Al. Our results, however, show that the Nd content was twice as high as the Al content, which may reveal a different charge compensation mechanism during the growth of zirconolite crystals from a glass matrix. In addition, the determination of chemical compositions for zirconolite crystals is highly beneficial for discussing their loading capacity of radionuclides, together with the partitioning ratio of radionuclides between crystalline and glass phases.

Symmetry Determination of Al–Nd Codoped Zirconolite in Zir GC and Zir PS. The LSI-indexing method implemented in the program TOPAS4.2 (Bruker AXS, 2009) was used to index the XRD patterns. On the basis of the crystal structures of five zirconolite polytypes,[13,17−20] the powder XRD pattern of the Zir-GC sample was found to match both zirconolite-2M (lower blue Miller indices in Figure 3; lattice parameters, a = 12.566 Å, b = 7.258 Å, c = 11.360 Å, and β = 100.66°) and zirconolite-3T (upper red Miller indices in Figure 3; lattice parameters, $a = b$ = 7.256 Å and c = 16.746 Å). To further confirm this outcome, SAED was used to limit the reflected diffraction signals to only those from the zirconolite crystals in the Zir-GC sample. The theoretical spacing distances for the 2M and 3T polytypes are shown in Table 1, and certain spacing values can be used to distinguish between the 2M and 3T structures, such as d = 5.252 Å for 2M and d = 5.026 Å for 3T (Table 1). As shown in Figure 4, d = 5.260 Å was observed in the SAED pattern of the zirconolite crystal in the Zir-GC sample. This value is close to the d = 5.252 Å in the 2M structure, which corresponds to the (−1−1−1) plane. Therefore, the structure of the zirconolite crystal in the Zir-GC sample can be identified as zirconolite-2M.

For the Zir-PS sample, with a trace of the perovskite phase, the zirconolite phase is major and its grain size is very large (>20 μm, in Figure 5). Its XRD pattern can be indexed based on a monoclinic unit cell with lattice parameters of a = 12.4836 Å, b = 7.2770 Å, c = 11.3811 Å, and β = 100.66°. The observed

DOI: 10.1021/acs.inorgchem.5b00847
Inorg. Chem. 2015, 54, 7353−7361

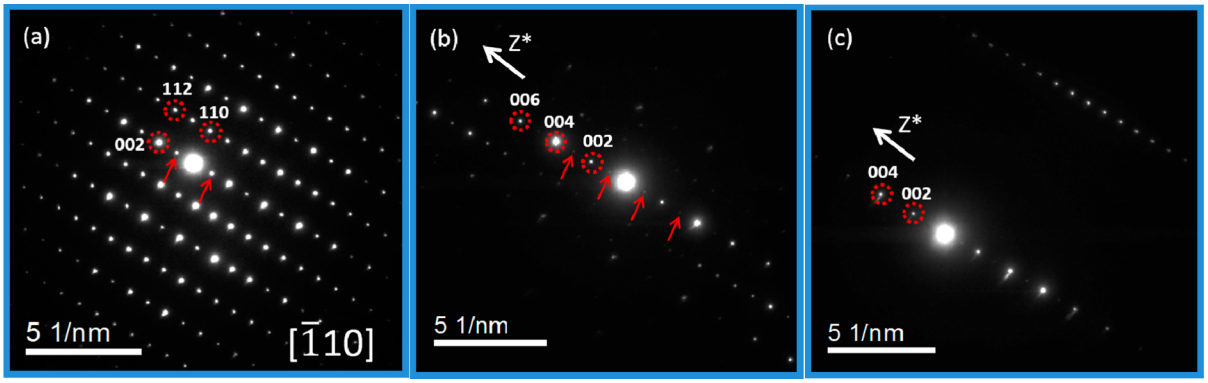

Figure 6. SAED pattern (a) along zone axis [-110] of the Al−Nd codoped zirconolite in the Zir-PS sample prepared by powder sintering at 1500 °C for a total of 100 h. When rotating the crystal about Z^*, the intensity of 00l reflections with l odd (indicated by arrows) decreased (b) and disappeared (c) due to double diffraction.

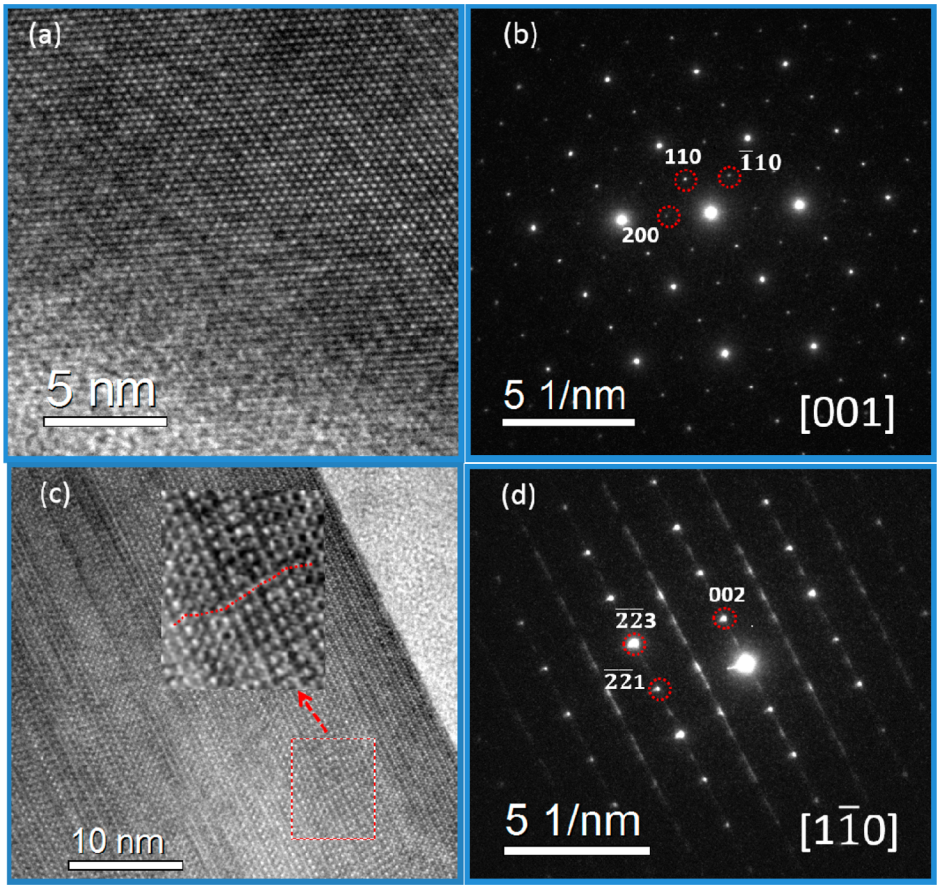

Figure 7. HRTEM image (a) and SAED pattern (b) of the Al−Nd codoped zirconolite in the Zir-GC sample presented along zone axis [001]. Along zone axis [1−10], the HRTEM image (c) and SAED pattern (d) reflect the dislocation feature in the sample.

extinction rules allow us to limit the possible space groups to $C2/c$ (no. 15) or Cc (no. 9). Among the five zirconolite structures, no structure was of the Cc (no. 9) space group, and the structures of zirconolite-4M and zirconolite-2M were of the $C2/c$ (no. 15) space group. It is interesting to note that the $Ca_{0.721}Nd_{0.494}Zr_{0.772}Ti_{1.997}O_7$ and $Ca_{0.479}Nd_{0.769}Zr_{0.716}Ti_{1.976}O_7$ compounds reported by Coelho et al.[19] had the same symmetry and similar lattice parameters (a, b, and β). Compared with the zirconolite-2M structure, both were assigned to the zirconolite-4M structure[19] due to a nearly double length along the c axis. A series of SAED patterns were used in the present study to further confirm the zirconolite structure in the Zir-PS sample. In Figure 6a, the spacing distance indicated by the red arrows is 11.30 Å. Considering that this spacing distance for the (002) planes (001 is forbidden in the $C12/c1$ (15) space group), the lattice parameter c is around 22.998 Å. This result is similar to that of the $Ca_{0.721}Nd_{0.494}Zr_{0.772}Ti_{1.997}O_7$ and $Ca_{0.479}Nd_{0.760}$-$Zr_{0.716}Ti_{1.976}O_7$ compounds, in which the lattice parameters of c were 22.987 and 23.081 Å, respectively. However, when the tilt experiments were carried out and the crystal was rotated about z^*, the intensity of the 00l reflections (with l of odd numbers) became strongly reduced (Figure 6b) and finally disappeared (Figure 6c). This result indicates that the appearance of spacing distance 11.30 Å and its corresponding 00l reflections, with l

DOI: 10.1021/acs.inorgchem.5b00847
Inorg. Chem. 2015, 54, 7353−7361

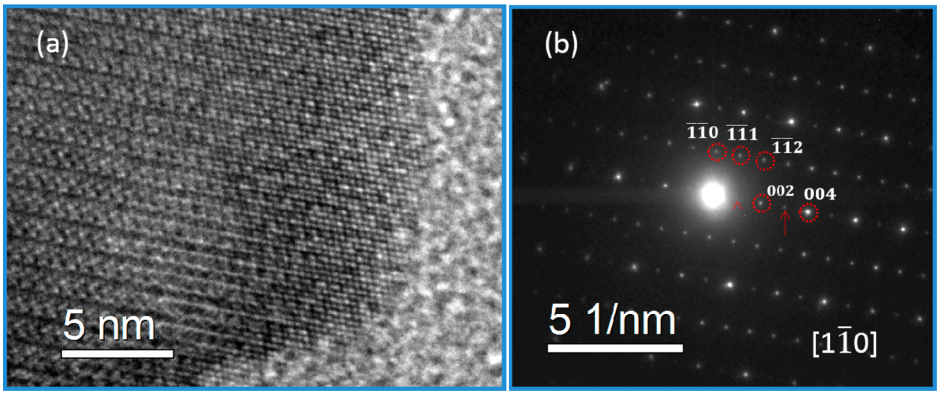

Figure 8. HRTEM image (a) of the Zir-PS sample and (b) its corresponding SAED pattern along zone axis [1−10]. The 00*l* reflections with *l* odd (indicated by arrows) are forbidden in the zirconolite-2M structure, but were still observed due to double diffraction.

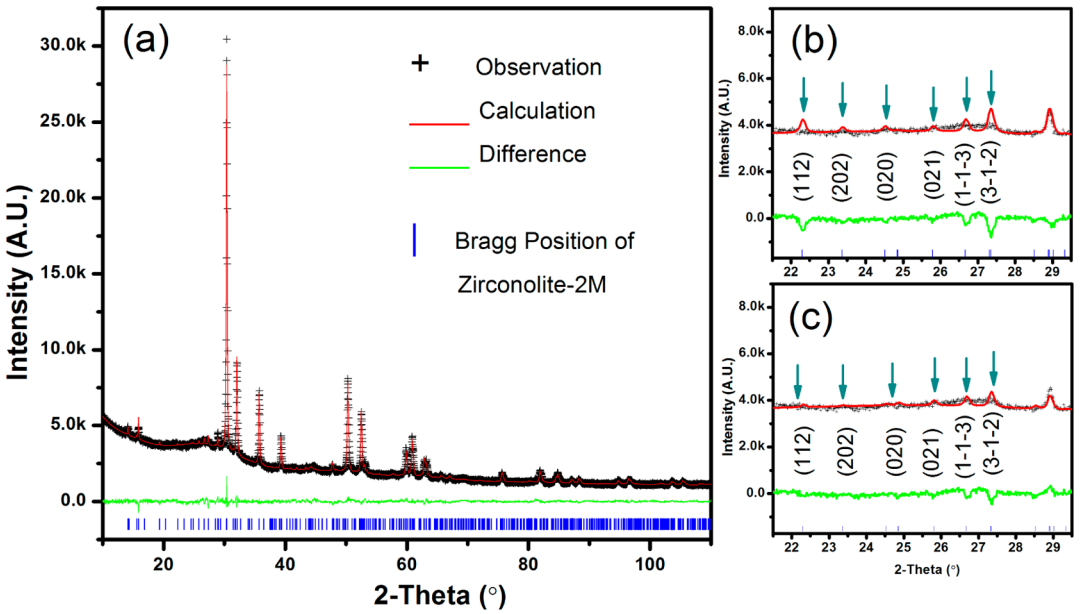

Figure 9. Structural Rietveld refinement result (a) for the Al−Nd codoped zirconolite in the Zir-GC sample. The details ranging from 21.5° to 29.5° show the diffraction planes of (112), (202), (020), (021), (1−1−3), and (3−1−2) before (b) and after (c) using the atom-split model.

odd numbers, is due to double diffraction.[26] Using the spots indicated with red circles, the SAED pattern can be indexed with zirconolite-2M in the [−110] direction (Figure 6a). This therefore confirms that the zirconolite derived from the Zir-PS sample is a zirconolite-2M structure rather than a zirconolite-4M structure.

Furthermore, although the structures of the zirconolite in both the Zir-GC and Zir-PS samples are zirconolite-2M, their XRD patterns are not identical. As can be seen from Figure S-1 in Supporting Information, a number of weak diffraction peaks observed in the Zir-PS sample do not occur in the pattern of the Zir-GC sample. In addition, the diffraction peaks of the Zir-GC sample generally show a broadening effect compared with those of the Zir-PS sample. Both diffraction peak characteristics indicate a need for further investigation of the structural details of zirconolite crystals derived from the Zir-GC sample.

Structural Details of Al−Nd Codoped Zirconolite in Zir-GC and Zir-PS. The lattice arrangement of Al−Nd codoped zirconolite prepared after nucleation at 810 °C for 2 h was clearly observed via HRTEM. No major distortions or lattice defects were observed (Figure 7a). The corresponding SAED pattern along zone axis [001] (Figure 7b) shows sharp and clear reflections. This result indicates that the atomic planes constructed along zone axis [001] are well ordered. Although the SAED pattern along zone axis [001] is similar to the 6-fold symmetry, it should be classified as the pseudohexagonal symmetry of the HTB layers. As discussed by White et al.,[27] the stacking angle of the HTB layers must be exactly 60° for the zirconolite-3T structure. As shown in Figure 7b, the angle between (−110) and (110) is 62.8°, and the angle between (110) and (200) is 57.6°. Therefore, this result further confirms that the zirconolite structure derived from the Zir-GC sample is zirconolite-2M, not zirconolite-3T.

Figure 6c and d show the HRTEM image and its corresponding SAED pattern in another zone axis direction. The HRTEM image also shows heavy dislocation of the lattice layers. The corresponding SAED pattern was indexed with the zirconolite-2M structure along the [1−10] zone axis based on clear reflections. Noticeable are serious streaks in this SAED pattern, which are parallel to the z^* direction and appear in $k = 2n - 1$reflections. The stacking faults in the lattice layers are considered the main contributor to these streaks.[28,29]

Additional HRTEM images and SAED patterns taken along the other directions are provided in Supporting Information

DOI: 10.1021/acs.inorgchem.5b00847
Inorg. Chem. 2015, 54, 7353−7361

Table 2. Structural Rietveld Refinement Results of the Al–Nd Codoped Zirconolite Phases for the Zir-GC Sample (Nucleation at 810 °C for 2 h and Crystal Growth at 1050 °C for 2 h) and the Zir-PS Sample (Powder Sintering at 1500 °C for a Total of 100 h)

site	Wyckoff	x	y	z	occupancy	Beq (Å^2)
Zir-GC: $Ca_{0.82}Nd_{0.23}Zr_{0.95}Ti_{1.87}Al_{0.13}O_7$, space group, $C12/c1(15)$; Z = 8; a = 12.562(1) Å; b = 7.2546 (6) Å, c = 11.3616 (3) Å; β = 100.67°; GOF = 1.42; R_{wp} = 2.96; R_p = 2.27						
Ca1	8	0.3718	0.1271	0.4932	0.69	0.51
Zr1	8	0.3716	0.1287	0.4930	0.13	0.72
Nd1	8	0.3608	0.1163	0.5084	0.18	0.24
Ca2	8	0.1199	0.1194	0.9807	0.13	0.17
Zr2	8	0.1205	0.1197	0.9854	0.82	1.83
Nd2	8	0.0981	0.1408	0.9511	0.05	0.36
Ti1	8	0.2469	0.1266	0.7481	1	0.76
Ti2	8	0.4816	0.0987	0.2528	0.37	0.35
Al1	8	0.4780	0.0766	0.2512	0.13	0.25
Ti3	4	0.0000	0.1194	0.25	1	0.40
O1	8	0.3586	0.1615	0.2764	1	1.76
O2	8	0.4849	0.1263	0.0887	1	1.85
O3	8	0.2245	0.1054	0.5857	1	0.06
O4	8	0.3790	0.1457	0.7110	1	1.02
O5	8	0.7195	0.1503	0.5818	1	0.25
O6	8	0.9952	0.1266	0.4112	1	2.29
O7	8	0.0880	0.0340	0.7748	1	0.36
Zir-PS: $Ca_{0.85}Nd_{0.24}Zr_{0.925}Ti_{1.755}Al_{0.23}O_7$, space group, $C12/c1(15)$; Z = 8; a = 12.4836(2) Å, b = 7.2770 (1) Å, c = 11.3811 (2) Å; β = 100.66°; GOF = 1.84; R_{wp} = 6.15; R_p = 4.55						
Ca1	8	0.3738	0.1274	0.4942	0.77	1.00
Nd1	8	0.3738	0.1274	0.4942	0.22	1.00
Zr1	8	0.3738	0.1274	0.4942	0.01	1.00
Ca2	8	0.1205	0.1232	0.9722	0.08	1.02
Nd2	8	0.1205	0.1232	0.9722	0.02	1.02
Zr2	8	0.1205	0.1232	0.9722	0.90	1.02
Ti1	8	0.2463	0.1280	0.7485	1	1.05
Ti2	8	0.4713	0.0546	0.2702	0.27	1.12
Al1	8	0.4713	0.0546	0.2702	0.23	1.12
Ti3	4	0.0000	0.1178	0.2500	0.97	1.00
Zr3	4	0.0000	0.1178	0.2500	0.03	1.00
O1	8	0.3092	0.1084	0.2791	1	1.59
O2	8	0.4682	0.1148	0.1074	1	0.59
O3	8	0.2017	0.0942	0.5775	1	1.01
O4	8	0.3856	0.1644	0.7113	1	1.58
O5	8	0.7190	0.1560	0.5903	1	0.79
O6	8	0.9903	0.1380	0.4068	1	0.36
O7	8	0.0947	0.0509	0.7975	1	1.80

(Figures S-2 and S-3) to further confirm the heavy stacking faults in the zirconolite crystals grown from a glass matrix. As indicated in ref 24 and 25, these stacking faults can enhance the radiation durability of zirconolite, so that their formation mechanism and atomic arrangements need to be investigated. According to electron diffraction theory,[30,31] diffuse streaks in reciprocal space may reveal a deviation of layer displacement from its ideal crystallographic site. Therefore, the above results indicate that the actual atomic planes are not strictly on the theoretical crystallographic planes. This information was used to construct a structural model of zirconolite crystals derived from a glass-ceramic matrix when carrying out the Rietveld refinement analysis.

Figure 8a and b shows the HRTEM image of the Zir-PS sample and its corresponding SAED pattern along zone axis [1−10]. The clear lattice fringes in the HRTEM image confirm the high-order crystallographic planes and highly crystalline nature of the Zir-PS sample. The corresponding SAED pattern in Figure 8b shows sharp diffraction spots. This SAED pattern also indicates a highly ordered structure, as these sharp diffraction spots in reciprocal space result from the well-arranged lattices in the sample.[31] The results of the HRTEM image and the SAED pattern indicate limited deviations in atomic arrangement from the theoretical crystallographic geometry. This information was also used in the Rietveld refinement analysis of the Al–Nd codoped zirconolite structure derived from the Zir-PS sample.

The broadening effect in the XRD pattern of the Zir-GC sample may also be caused by the heavy stacking faults in the zirconolite crystals. In general, the small crystal size (<100 nm) and substantial lattice defects (due to kinematical scattering) are mainly responsible for the broadening effect in XRD patterns.[32] However, the crystal size of the Zir-GC sample was confirmed as 100−500 nm (Figure 1). The broadening effect in the peaks observed in this sample is thus mainly due to the observed lattice defects rather than the stacking faults.

Rietveld Refinement of Al–Nd Codoped Zirconolites. The XRD pattern obtained from the Zir-GC sample was further used for the Rietveld refinement analysis (Figure 9). The zirconolite-2M $Ca_{0.85}Nd_{0.15}Ti_{2.15}Zr_{0.85}O_7$[33] crystal data were used as the initial structure model of the zirconolite crystals. Loiseau et al.[8] pointed out that disorder in the Zr/Ca layers would lead to a decrease in intensity of some peaks in the XRD pattern. However, the initial step in adopting this assumption in the Rietveld refinement process failed to generate a satisfactory fitting outcome. The modeled peak intensities of the (112), (202), (020), (021), (1−1−3), and (3−1−2) planes were still significantly higher than those observed from the XRD data (Figure 9b). This finding indicates that the disorder of the Zr/Ca layers is not the main cause of the observed diffraction pattern. Through the SAED and HRTEM results, substantial stacking faults were found in these crystals, and thus a significant peak-broadening effect should be further considered. To describe the zirconolite crystal structure in the Zir-GC sample, a split-atom model was thus introduced, which has been successfully used to solve the distorted structures of other compounds.[34−36] In general, the split-atom model is implemented by decreasing the Wyckoff site symmetry or splitting one site into more than two fractions.[34−36] In the zirconolite-2M structure, the lowest Wyckoff site symmetry is the 8f site, and its symmetry cannot be further decreased in this structure. Therefore, the method of splitting one site into more than two fractions was used in our analysis.

As oxygen atoms often make only a limited contribution to XRD peak intensity, the sites occupied by oxygen atoms were not split, and only the 8f sites occupied by cations were split. In the split-atom model, the 8f site in the CaO_8 octahedron was split into three fractions, and these were occupied by Ca^{2+}, Zr^{4+}, and Nd^{3+} ions. The 8f site in the ZrO_7 polyhedron was also split into three fractions occupied by Ca^{2+}, Zr^{4+}, and Nd^{3+} ions. Only half of the 5-coordinated Ti sites are available for cations in the zirconolite-2M structure, and these sites were split into two fractions for Ti^{4+} and Al^{3+} ions. The occupancies of different cations in CaO_8, ZrO_7, and the half-occupied TiO_5 polyhedra were subject to the charge compensation constraint in the Rietveld refinement analysis. The fundamental parameters approach was performed to simulate the peak shape in the Rietveld refinement analysis. The refined

DOI: 10.1021/acs.inorgchem.5b00847
Inorg. Chem. 2015, 54, 7353−7361

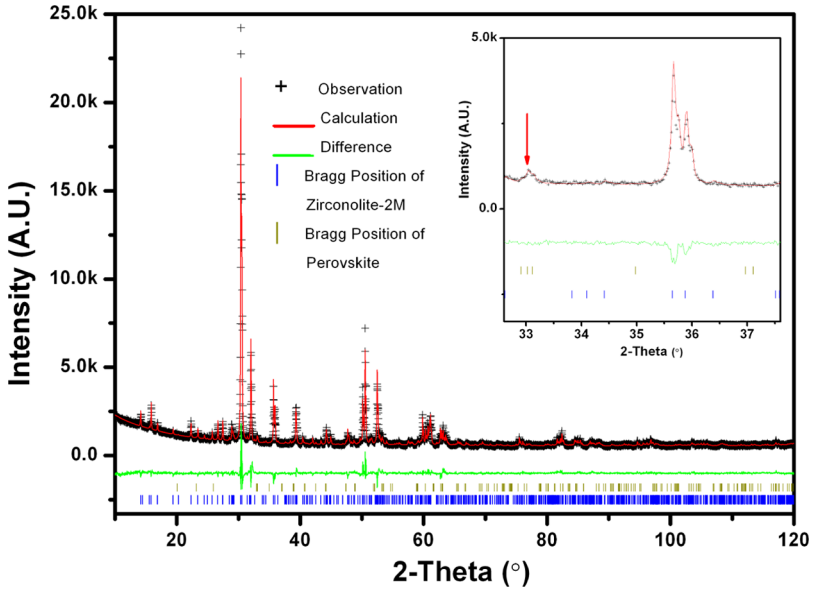

Figure 10. Structural Rietveld refinement result of the Al–Nd codoped zirconolite in the Zir-PS sample. The inset shows details of the range 32.5° to 37.7° and the red arrow indicates the main peak of the perovskite phase.

parameters included scale factor, specimen displacement, background, lattice parameters, crystallite sizes, microstrain, occupancy, atomic positions, and atomic displacement parameters. Figure 9a shows the results of the Rietveld refinement fitted for the powder diffraction pattern of the Zir-GC sample. The simulated pattern fits well with the experimental data, and the R_{wp}, R_p, and goodness of fit (GOF) values are 2.96, 2.27, and 1.42, respectively. The low values of these parameters indicate the high quality of this structure simulation result. The fitting details in Figure 9c show that the calculated intensities of the (112), (202), (020), and (021) planes were nearly at the background levels and that the intensities of the (1−1−3) and (3−1−2) planes were also further reduced with the atom-split model. The parameters derived by the Rietveld refinement analysis are summarized in Table 2. The success of describing the crystal structure with extensive stacking faults through the atom-split model provides the precise atomic arrangements of zirconolite. These structural details are helpful for predicting the radiation tolerance of zirconolite crystals in glass-ceramic. Such information is crucial for the molecular dynamics simulation work, which is primarily used for estimating the stability of immobilized products after hundreds of years.

On the basis of the refinement result for the site occupancies, the Al–Nd codoped zirconolite grown from the glass matrix can be expressed as $Ca_{0.82}Nd_{0.23}Zr_{0.95}Ti_{1.87}Al_{0.13}O_7$ (Table 2). This outcome in general agrees with the TEM-EDX result of $Ca_{0.83}Nd_{0.25}Zr_{0.85}Ti_{1.95}Al_{0.11}O_7$. Most (nearly 80%) of the Nd^{3+} preferentially occupied the CaO_8 octahedra, while the remainder entered the ZrO_7 polyhedra. This is consistent with the results concluded from low temperature optical absorption spectra and electron spin resonance spectra for glass-ceramic zirconolite samples.[7,9] In those reports, two neodymium incorporation mechanisms (i.e., (Nd^{3+}, Al^{3+}) ↔ (Ca^{2+}, Zr^{4+}) and (Nd^{3+}, Nd^{3+}) ↔ (Ca^{2+}, Zr^{4+})) were proposed when Nd_2O_3 is larger than 4 wt %. This study further confirmed these two mechanisms through the Rietveld refinement result, and thus, the split-atom model is proven to be helpful in the construction of the zirconolite structures derived from the glass matrix.

Two crystalline phases, zirconolite-2M ($Ca_{0.85}Nd_{0.15}Ti_{2.15}Zr_{0.85}O_7$)[33] and perovskite ($CaTiO_3$),[37] were identified from the XRD pattern of the Zir-PS sample. Perovskite was a trace phase in this sample, as shown by its low-intensity peaks in the pattern (inset in Figure 10) and was quantified as only around 1.9 wt %. The split-atom model was not used for the zirconolite-2M structure, as no substantial lattice defects were observed in this zirconolite crystal, as shown by the HRTEM and SAED results. In the Rietveld refinement analysis, Al^{3+} was assigned to the split five-coordinated Ti site as described by Loiseau et al.[6] The simulated pattern fits well with the experimental data, and the obtained agreement indices are R_{wp} = 6.15, R_p = 4.55, and GOF = 1.84. The values of these parameters are low and indicate a quality refinement result for the Zir-PS sample (Figure 10). The codoped zirconolite structural framework and its site occupancies derived from Rietveld refinement analysis are summarized in Table 2. This zirconolite can be expressed as $Ca_{0.85}Nd_{0.24}Zr_{0.925}Ti_{1.755}Al_{0.23}O_7$ based on the refinement result. Most (nearly 90%) of the Nd^{3+} cations occupy the Ca sites, while the remaining ones enter the Zr sites. The preference for occupying the Ca sites is likely to be due to the similar ionic radii of Nd^{3+} (r = 1.109 Å) and Ca^{2+} (r = 1.12 Å) compared to that of Zr^{4+} (r = 0.84 Å).[6]

CONCLUSIONS

The chemical composition and crystal structure of Al–Nd codoped zirconolite grown from a CaO-SiO_2-Al_2O_3-TiO_2-ZrO_2-Nd_2O_3-Na_2O glass matrix at 1050 °C were analyzed for the first time. The crystal structure of zirconolite $Ca_{0.85}Nd_{0.24}Zr_{0.925}Ti_{1.755}Al_{0.23}O_7$ prepared by powder sintering was also determined. Through a TEM-EDX technique, the chemical composition of the Al–Nd codoped zirconolite crystal grown from glass was determined to be $Ca_{0.83}Nd_{0.25}Zr_{0.85}Ti_{1.95}Al_{0.11}O_7$. Combining the PXRD and SAED results revealed that both of these Al–Nd codoped zirconolite phases were crystallized in the zirconolite-2M structure (space group $C12/c1$, no. 15). The lattice parameters of the Al–Nd codoped

DOI: 10.1021/acs.inorgchem.5b00847
Inorg. Chem. 2015, 54, 7353−7361

zirconolite grown from glass and prepared by powder sintering are a = 12.562(1) Å, b = 7.2546 (6) Å, c = 11.3616 (3) Å, and β = 100.67°; and a = 12.4836(2) Å, b = 7.2770 (1) Å, c = 11.3811 (2) Å, and β = 100.66°, respectively. The extensive SAED tilt experiments confirmed that the appearance of spacing distance (11.30 Å) is due to the double diffraction. In the HRTEM images and SAED results, heavy stacking faults were commonly found in the Al−Nd codoped zirconolite grown from glass but not in that obtained by powder sintering. The atom-split model was introduced for the first time in the Rietveld refinement, and this successfully described the crystal structure of zirconolite grown from glass, even under the strong influence of stacking faults in zirconolite. The overall result indicates that in both zirconolite products the majority of Nd^{3+} ions prefer to occupy the CaO_8 octahedra, while the rest enter the ZrO_7 polyhedra.

■ ASSOCIATED CONTENT

Supporting Information

XRD pattern of the Zir-GC and Zir-PS sample; HRTEM image (left) and SAED pattern (right) of the Al−Nd codoped zirconolite in the Zir-GC sample presented along zone axis [−1−54]; and SAED pattern of the Al−Nd codoped zirconolite in the Zir-GC sample presented along zone axis [−341]. The Supporting Information is available free of charge on the ACS Publications website at DOI: 10.1021/acs.inorgchem.5b00847.

■ AUTHOR INFORMATION

Corresponding Author

*E-mail: kshih@hku.hk.

Notes

The authors declare no competing financial interest.

■ ACKNOWLEDGMENTS

We thank Frankie Y. F. Chan for his help with the TEM experiments and the discussion. We gratefully acknowledge the funding for this research provided by the General Research Fund Scheme of the Research Grants Council of Hong Kong (715612, 17206714), HKU Strategic Research Themes on Clear Energy and Earth as a Habitable Planet, and the Centre for Nuclear Engineering at Imperial College London.

■ REFERENCES

(1) Ewing, R. C. *Can. Mineral.* **2001**, *39*, 697−715.
(2) Lee, W. E.; Ojovan, M. I.; Stennett, M. C.; Hyatt, N. C. *Adv. Appl. Ceram.* **2006**, *105*, 3−12.
(3) Ojovan, M. I.; Lee, W. E. *An Introduction to Nuclear Waste Immobilisation*, 2nd ed.; Elsevier: Amsterdam, The Netherlands, 2014.
(4) Ojovan, M. I.; Lee, W. E. *Metall. Mater. Trans. A* **2011**, *42*, 837−851.
(5) Burakov, B. E.; Ojovan, M. I.; Lee, W. E. *Crystalline Materials for Actinide Immobilisation*; Imperial College Press: London, UK, 2011.
(6) Loiseau, P.; Caurant, D.; Baffier, N.; Fillet, C. *Materials Research Society Symposium - Proceedings* **2003**, 243−250.
(7) Loiseau, P.; Caurant, D.; Baffier, N.; Fillet, C. *Mater. Res. Soc. Symp. Proc.* **2001**, 169−177.
(8) Loiseau, P.; Caurant, D.; Baffier, N.; Mazerolles, L.; Fillet, C. *Mater. Res. Soc. Symp. Proc.* **2001**, 179−187.
(9) Loiseau, P.; Caurant, D.; Baffier, N. *Phys. Chem. Glasses* **2002**, *43C*, 201−206.
(10) Loiseau, P.; Caurant, D.; Baffier, N.; Mazerolles, L.; Fillet, C.; Caurant, D. *J. Nucl. Mater.* **2004**, *335*, 14−32.
(11) Loiseau, P.; Caurant, D. *J. Nucl. Mater.* **2010**, *402*, 38−54.
(12) Whittle, K. R.; Hyatt, N. C.; Smith, K. L.; Margiolaki, I.; Berry, F. J.; Knight, K. S.; Lumpkin, G. R. *Am. Mineral.* **2012**, *97*, 291−298.
(13) Rossell, H. J. *Nature* **1980**, *283*, 282−283.
(14) Lumpkin, G. R. *Elements* **2006**, *2*, 365−372.
(15) Yudintsev, S. V.; Stefanovsky, S. V.; Ewing, R. C. Actinide Host Phases as Radioactive Waste Forms. In *Structural Chemistry of Inorganic Actinide Compounds*; Krivovichev, S. V., Burns, P. C., Tananaev, I. G., Eds.; Elsevier: Amsterdam, The Netherlands, 2007; pp 457− 490.
(16) Bayliss, P.; Mazzi, F.; Munno, R.; White, T. J. *Mineral. Mag.* **1989**, *53*, 565−569.
(17) Grey, I. E.; Mumme, W. G.; Ness, T. J.; Roth, R. S.; Smith, K. L. *J. Solid State Chem.* **2003**, *174*, 285−295.
(18) Mazzi, F.; Munno, R. *Am. Mineral.* **1983**, *68*, 262−276.
(19) Coelho, A. A.; Cheary, R. W.; Smith, K. L. *J. Solid State Chem.* **1997**, *129*, 346−359.
(20) Cheary, R. W.; Coelho, A. A. *Phys. Chem. Miner.* **1997**, *24*, 447−454.
(21) Triyacharoen, P. *Phase Stability of Zirconolite Cation Substitution for Immobilization of Actinides*; Michigan Technological University: Houghton, MI, 2003.
(22) Loiseau, P.; Caurant, D.; Majerus, O.; Baffier, N.; Mazerolles, L. *Phys. Chem. Glasses* **2002**, *43*, 195−200.
(23) Loiseau, P.; Caurant, D.; Majerus, O.; Baffier, N. *J. Mater. Sci.* **2003**, *38*, 843−852.
(24) Shen, T. D. *Nucl. Instrum. Methods Phys. Res., Sect. B* **2008**, *266*, 921−925.
(25) Mulroue, J.; Watkins, M.; Morris, A. J.; Duffy, D. M. *J. Nucl. Mater.* **2013**, *437*, 261−266.
(26) Champness, P. E. *Electron Diffraction in the Transmission Electron Microscopy*; Bios Scientific Publishers: Oxford, UK, 2001.
(27) White, T. J. *Am. Mineral.* **1984**, *69*, 1156−1172.
(28) Ho, G. W.; Wong, A. S. W.; Kang, D.-J.; Welland, M. E. *Nanotechnology* **2004**, *15*, 996−999.
(29) Dai, H.; Wong, E. W.; Lu, Y. Z.; Fan, S.; Lieber, C. M. *Nature* **1995**, *375*, 769−772.
(30) Hirsch, P. B.; Howie, A.; Nicholson, R. B.; Pashley, D. W.; Whelan, M. J. *Electron Microscopy of Thin Crystals*, 1st ed.; Butterworth & Co.: London, UK, 1967.
(31) Van Tendeloo, G.; Amelinckx, S. *Phase Transitions* **1998**, *67*, 101−135.
(32) Ungár, T. *Scr. Mater.* **2004**, *51*, 777−781.
(33) Rossell, H. J. *J. Solid State Chem.* **1992**, *99*, 38−51.
(34) Belik, A. A.; Izumi, F.; Stefanovich, S. Y.; Malakho, A. P.; Lazoryak, B. I.; Leonidov, I. A.; Leonidova, O. N.; Davydov, S. A. *Chem. Mater.* **2002**, *14*, 3197−3205.
(35) Izumi, F. *Solid State Ionics* **2004**, *172*, 1−6.
(36) Fukuda, K.; Ito, M.; Iwata, T. *J. Solid State Chem.* **2007**, *180*, 2305−2309.
(37) Ali, R.; Yashima, M. *J. Solid State Chem.* **2005**, *178*, 2867−2872.

DOI: 10.1021/acs.inorgchem.5b00847
Inorg. Chem. 2015, 54, 7353−7361